**Proceedings Paper:**
Waddoups, R. orcid.org/0000-0002-2241-3784, Clarke, S., Curry, R. et al. (6 more authors) (2024) Validation of numerical modelling of explosive ground shock propagation in dry sand with digital image correlation experiments. In: Proceedings of The 19th International Symposium on Interaction of the Effects of Munitions with Structures (ISIEMS). 19th International Symposium on Interaction of the Effects of Munitions with Structures (ISIEMS), 09-13 Dec 2024, Bonn, Germany. International Symposium on Interaction of the Effects of Munitions with Structures (ISIEMS)

eprints@whiterose.ac.uk
https://eprints.whiterose.ac.uk/

# Validation of Numerical Modelling of Explosive Ground Shock Propagation in Dry Sand with Digital Image Correlation Experiments

**Ross Waddoups[1,2,*], Sam Clarke[1,2], Richard Curry[1], Andy Tyas[1,2], Dain Farrimond[1,2], Adam Dennis[1], Tommy Lodge[1,2], Joshua Mullins[3], Joseph Cordell[3]**

1 School of Mechanical, Aerospace and Civil Engineering, University of Sheffield, Mappin Street, Sheffield, S1 3JD, UK

2 Blastech Ltd., The Innovation Centre, 217 Portobello, Sheffield, S1 4DP, UK

3 Defence Science and Technology Laboratory (Dstl), Porton Down, Salisbury, SP4 0JQ, UK

**Abstract**

Explosions from buried charges generate compressive stress waves, commonly referred to as ground shock, which displace and accelerate structures located both underground and on the surface. In this study, the effects of ground shock on a simplified buried structure have been recorded experimentally through digital image correlation from stereo high-speed video cameras at one hundred thousand frames per second, with this used to validate a numerical model.

This testing utilised a steel pipe with a clamped aluminium base plate (to represent a deformable structure), filled with varying depths of Leighton Buzzard sand. From the DIC data, displacement-time histories were extracted from an area of 380 x 160mm of the base plate (approximately 3500 individual locations), allowing for high spatial and temporal resolutions for comparison against modelled outputs.

Numerical modelling in LS-Dyna, utilising an MMALE scheme, was found to capture the shock propagation well, with good agreement between experimental and numerical findings, particularly at close stand-offs. As stand-off increased, mass soil movement had a larger influence on deformation of the structure, which the model struggled to capture effectively.

## Introduction

Explosions in the ground can cause damage to buried infrastructure and building substructures, as well as causing potential injury or death. There were a total of approximately 17kT of bombs dropped on London in World War Two; an estimated ten percent of these remained as unexploded ordnance (UXO) [1]. It is suggested that over twenty times the amount of bombs were dropped on Germany compared to Britain [2] (e.g. in Figure 1), leading to UXO continuing to pose a serious risk across the world. Today, many construction projects are affected by the presence of UXO, with guidance on mitigating UXO risks introduced by the UK construction sector for all construction sites in 2009 [2]. Thus, there is a clear need to be able to understand and model the transmission of ground shock to buried structures, to enable effective mitigation if UXO is found.



**Figure 1.** Unexploded WWII bomb found in 2011 in Koblenz, Germany
(Holger Weinandt, CC BY-SA 3.0 DE <https://creativecommons.org/licenses/by-sa/3.0/de/deed.en>, via Wikimedia Commons)

Much early work was done to characterise ground shock using large scale experimental tests [3, 4, 5], with historic and recent work conducted on the development of sensors to effectively measure ground shock [6, 7, 8]. Empirical predictive formulae were developed to describe the measured phenomena [9, 10, 11, 12], allowing for the prediction of free-field in-ground loading at a single point – as implemented in TM5-855-1 Fundamentals of Protective Design for Conventional Weapons [13].

Additionally, work has been done in the development of numerical models which can represent the transmission of loading from an explosion through soil. Laine and Larsen [14] used Autodyn to model varied soil types and characterise the coupling behaviour as a result of burial depth for each of these. Laine et al. [15, 16, 17] later modelled the experimental testing of Hultgren [18] in order to understand the distribution of energy within the system. From this, it was found that the loading could not be described as purely impulsive, with the mass of soil between the charge and a structure strongly influencing the loading. Shelton [19] also investigated the coupling of the explosive energy with the ground through both numerical modelling and experimental results, suggesting that the coupling factors described in TM5-855-1 [13] lead to a lower-bound estimate of peak stress and peak particle velocity.

Although a wealth of tests and models exist, high-resolution spatial distributions of ground shock on a buried structure are lacking, with a dedicated experimental approach required to validate predictive numerical models. Therefore, this paper describes a study undertaken to effectively capture the spatial and temporal distribution of ground shock on a structure underground, validating numerical modelling which builds upon the work described previously.

## Methodology

### Experimental Procedure

In order to capture the spatial distribution of loading on a structure, a 3D Digital Image Correlation (DIC) technique was utilised with a pair of Photron SA-Z high speed video (HSV) cameras. This allowed for displacement data to be captured across an area of 640 x 280 pixels over 380mm x 160mm of a 3mm thick AL-6082-T6 plate. This plate, clamped in the base of a 592mm diameter steel pipe soil container, represented a simplified buried structure, with a varying depth of soil placed within the container. A constant depth of burial (DOB) from the soil surface to a 10g spherical PE10 charge was maintained, with the stand-off distance (SOD) varied throughout the test series. This setup is outlined in Figure 2.
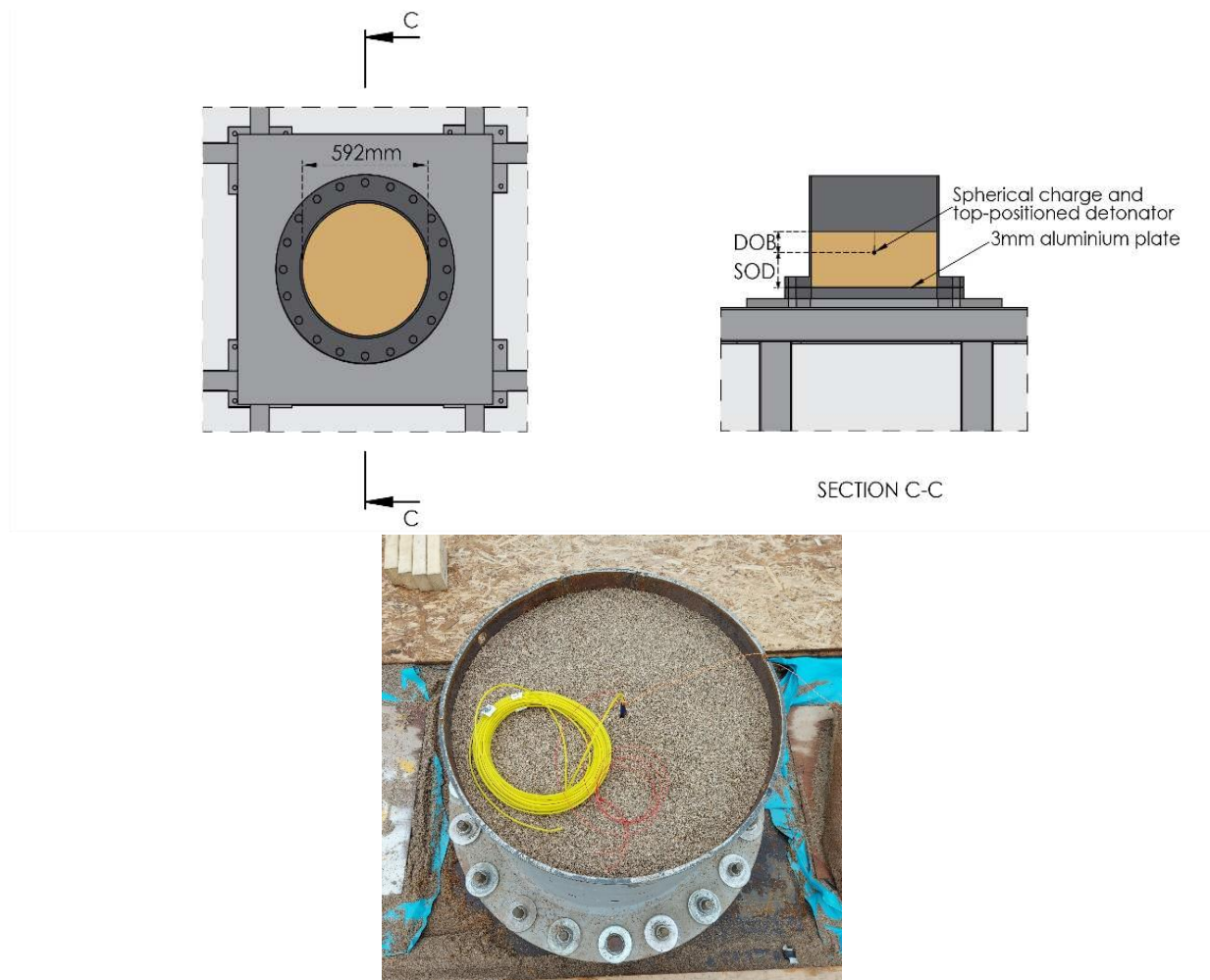


**Figure 2.** Soil container with aluminium baseplate

Uniform Leighton Buzzard 14/25 sand (LB) with a bulk density of $1.65g/cm^3 \pm 0.01g/cm^3$ and a moisture content of $5\% \pm 0.2\%$ was utilised for all tests, in order to ensure a consistent transmission medium. LB has previously been found to contribute to a consistent, repeatable loading behaviour within blast experiments [20, 21], leading to it being selected as a suitable material for this work. LB is characterised as a uniform sand with a $D_{60}$ of 0.9mm and a $D_{10}$ of 0.7mm.

The two HSV cameras were positioned below the soil container at 15 degrees from vertical (an included angle of 30 degrees) on a frame which was isolated from the main support structure to reduce the influence of in-structure vibrations (as shown in Figure 3). The cameras were positioned 1800mm from the target plate, utilizing matching 50mm lenses at an aperture of f/4. Recordings were made at one hundred thousand frames per second, allowing for a high temporal resolution to be achieved from a total of approximately 3500 locations across the plate.
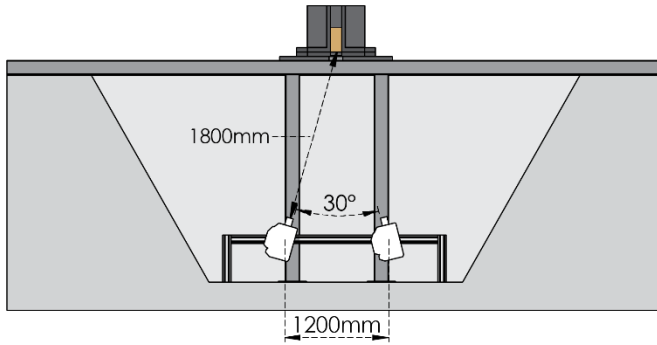
**Figure 3.** Experimental apparatus with soil container supported above HSV cameras

The results of three tests are discussed herein, according to the details in Table 1. These covered a large range of SOD, representing equivalent distances of 0.22m – 2.17m for a 1kg charge according to cube-root scaling (established by Lampson [3] for ground shock propagation).

| Charge Mass [g] | SOD [mm] | DOB [mm] | Scaled SOD [m/kg$^{1/3}$] | Bulk Density [g/cm$^3$] | Moisture Content [%] |
|---|---|---|---|---|---|
| 10 | 50 | 100 | 0.22 | 1.652 | 5.12 |
| 10 | 250 | 100 | 1.09 | 1.649 | 5.04 |
| 10 | 500 | 100 | 2.17 | 1.645 | 4.84 |

**Table 1.** Experimental test details

## Numerical Modelling

The experiment was modelled using a 2D axisymmetric Multi-Material Arbitrary Lagrange Eulerian (MMALE) approach in LS-DYNA (as in Figure 4). Reflective boundaries were used with a vacuum (MAT_VACUUM_TITLE) above and below the region of interest to allow the soil and plate to move freely without reflected air shocks or damping effects contributing to the response. A 1mm cell size was selected for the ALE region and plate, and a 2mm cell size for the steel clamps.

A MAT_PSEUDO_TENSOR was used for the soil with an EOS_TABULATED_COMPACTION utilising the values found by Laine & Sandvik [22] for Sjöbo sand at an average bulk density of 1.674g/cm$^3$ and moisture content of 6.57%. The aluminium plate and steel clamps were modelled using MAT_SIMPLIFIED_JOHNSON_COOK with parameters sourced from Chen et al. [23] and Vedantam et al. [24] respectively, with the surface friction modelled using CONTACT_2D_AUTOMATIC_ SURFACE_TO_SURFACE. The PE10 explosive was modelled as a MAT_HIGH_EXPLOSIVE_BURN with an EOS_JWL.

Before reaching this final model setup, various simplified versions were trialled to reduce the model complexity and associated runtime. With each iteration, the plate response was assessed against the experimental findings, until the optimum setup was found. The changes made through this process were as follows:

- Change from fixed nodes at plate edge to modelling of full clamp structure (resulted in better plate response by slowing vibration due to an increased effective length)
- Trialling of various boundary conditions for the ALE domain (non-reflective resulted in instabilities, and undefined outflow boundaries caused reflected shocks to interfere with the response)
- Replacement of air in the ALE domain with a vacuum (resulted in the removal of reflected shocks from boundaries and piston-type damping effects)

Each of the tested SODs was modelled, with the domain extended vertically to allow for the constant DOB to be maintained. Displacement-time histories were extracted from each node along the plate, to allow for comparison against the experimentally-derived data, allowing for validation of the model. This ensures that in-soil quantities (such as pressure distributions, as in Figure 5) can be extracted from soil-structure interaction events across a range of SODs.
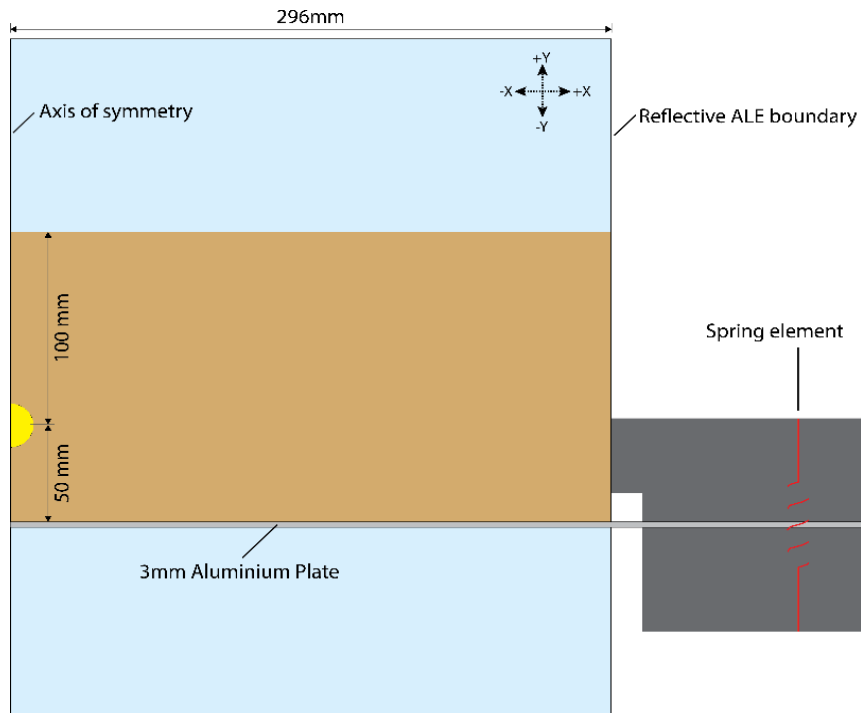


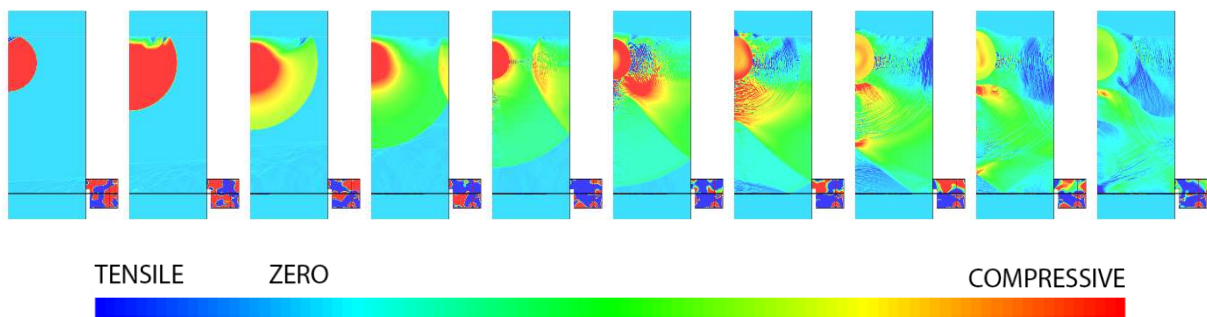**Figure 4.** Numerical model setup for the 50mm SOD test



**Figure 5.** Modelled pressure distribution through the soil for a 500mm SOD test over 2ms

## Surface Deformation

As already described, like-for-like comparisons of the plate deformation can be made between the model and corresponding experiments. This can be done by taking a line-slice of data across the long axis of the DIC window (for the length of the recording) and comparing it against the 2D axisymmetric plate displacement in the model. In Figure 6, it can be seen that the load transfer at 50mm SOD ($0.22\text{m/kg}^{1/3}$) results in an accurate representation of initial displacement across the plate within the model, with largely similar magnitudes of displacement throughout the modelled time.
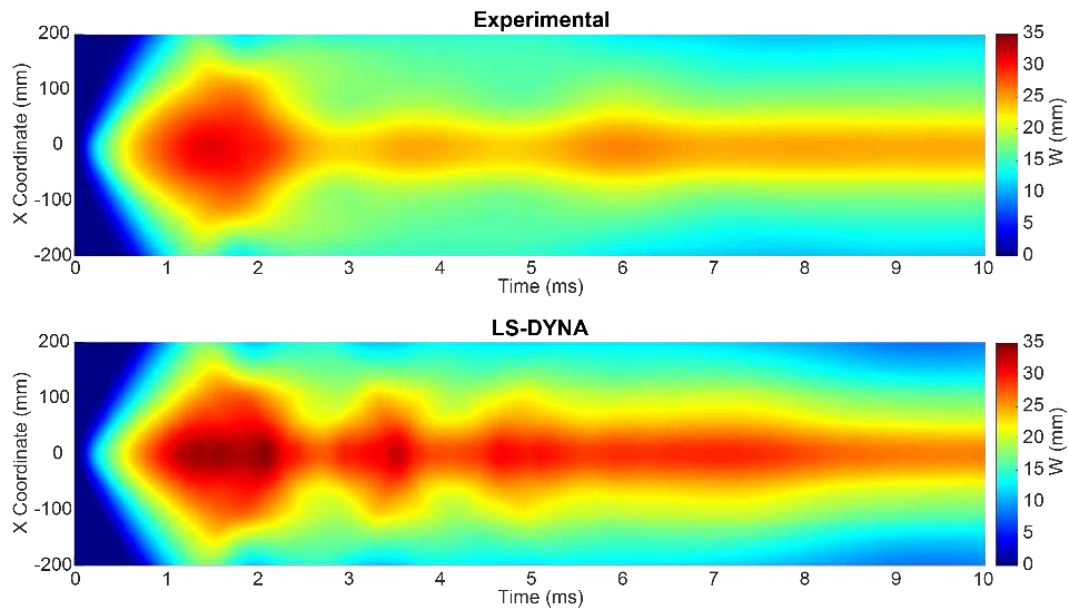


**Figure 6.** Experimental and modelled displacement for 50mm SOD

As SOD is increased to 250mm ($1.09\text{m/kg}^{1/3}$) in Figure 7, the time of arrival of the loading can be seen to be largely similar between the model and experiment, however the displacement profile is more centralised in the experimental results than in the model. The magnitude of displacement is generally the same, however the time of peak displacement is later in the model than seen in the experiment.
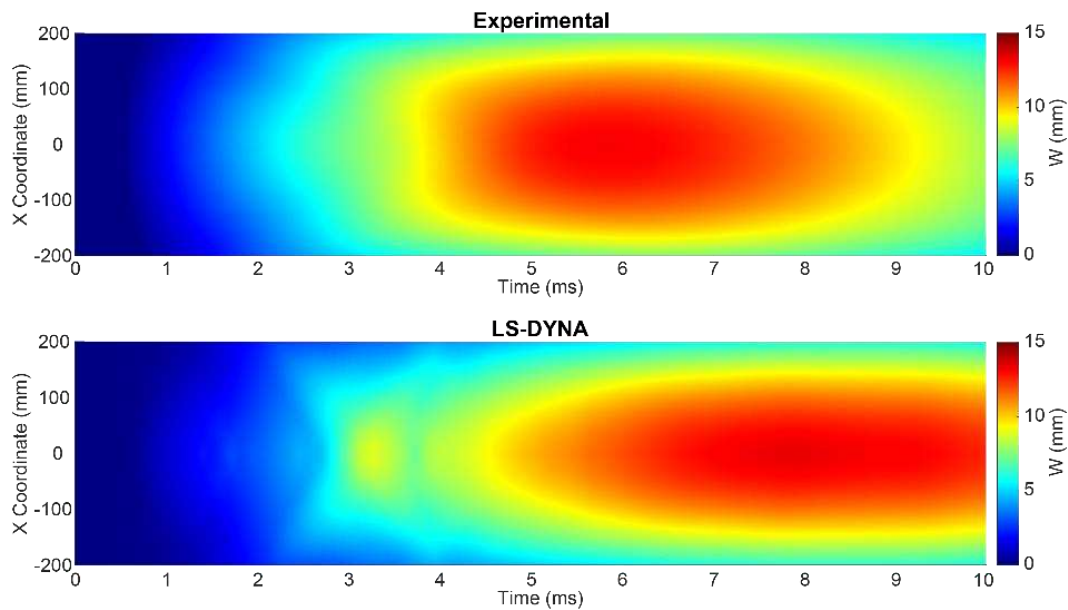


**Figure 7.** Experimental and modelled displacement for 250mm SOD

6

In Figure 8, further increasing the SOD to 500mm (2.17m/kg$^{1/3}$), it can be seen that the model deviates significantly from the experimental findings. The time of arrival of the initial load is similar, however the plate response is significantly different. The peak displacement magnitude can be seen to be similar, however the modelled plate responds far faster than the experiment, reaching a peak magnitude significantly more quickly before vibrating. In contrast, the plate in the experiment is displaced more slowly with little vibration.
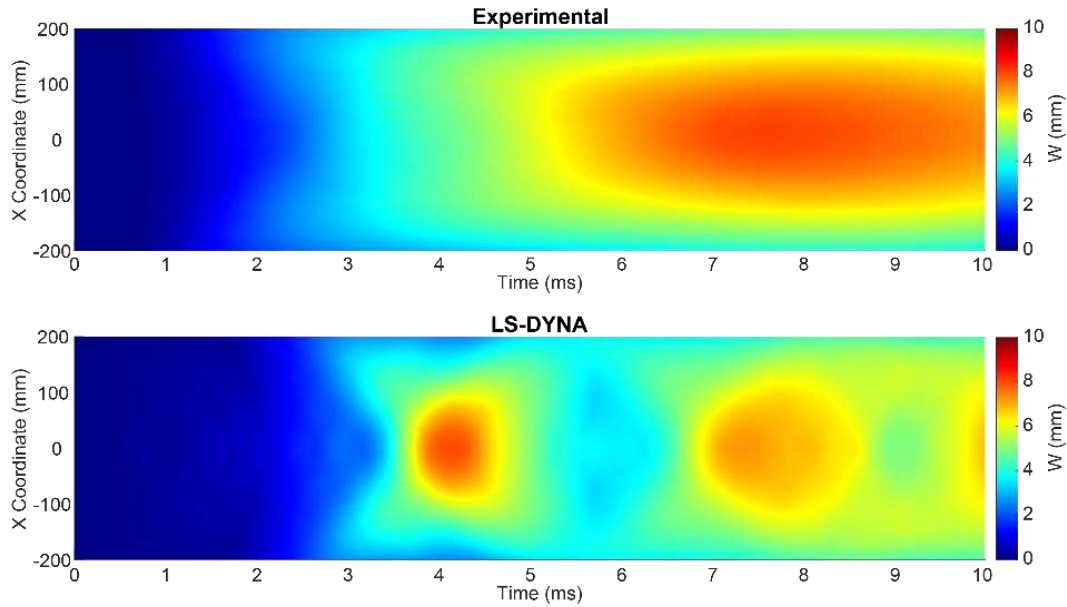


**Figure 8.** Experimental and modelled displacement for 500mm SOD

## Midpoint Displacement

Refining the comparison to the midpoints of each of the plates in Figure 9 further illustrates the difference in plate response between the experiment and model. It can be seen that the model effectively captures the peak magnitude of displacement across the SOD range (with an average error of 10% at the plate midpoint). Additionally, for the 50mm and 250mm SOD cases, the model can be seen to acceptably capture the plate behaviour after the initial shock loading. However, as the SOD increases, the model fails to effectively capture the long-term plate movement. It is believed that this is likely due to the model allowing for the transfer of ground shock loading to the plate, without the continued movement of the soil against the plate – leading to an undamped response.
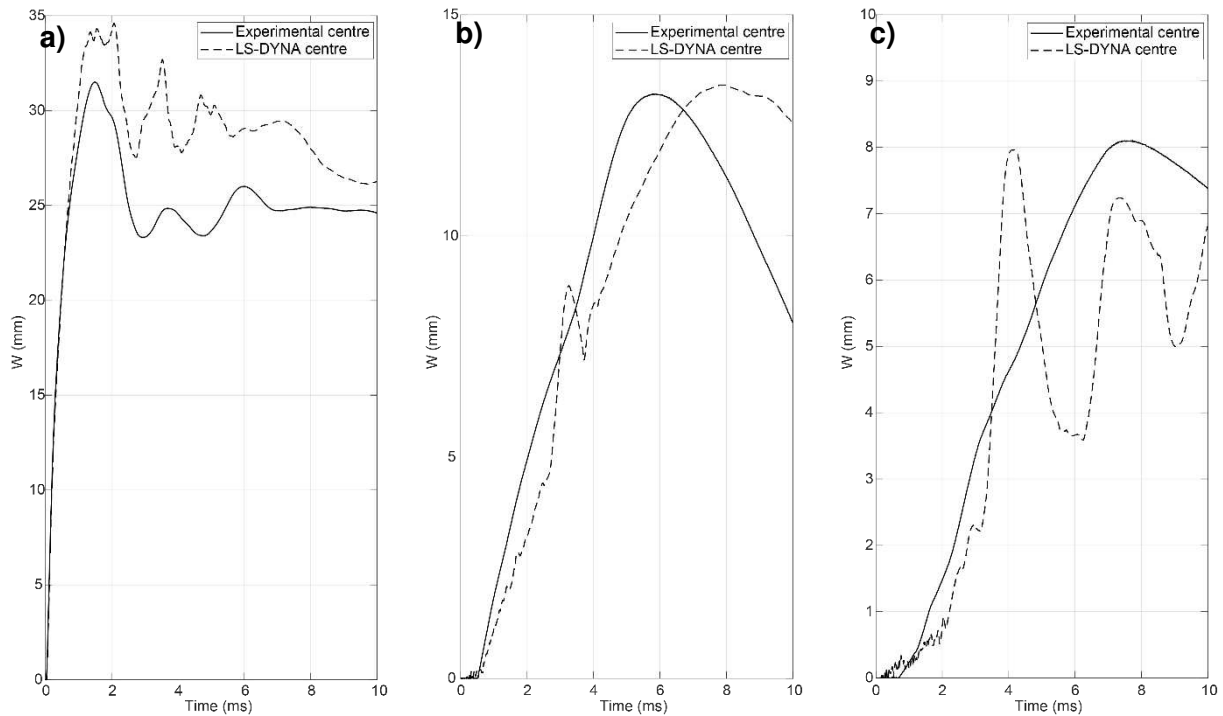
7

**Figure 9.** Midpoint displacement of experimental and modelled plates:
a) 50mm SOD, b) 250mm SOD, c) 500mm SOD

This agrees with the findings of Laine et al. [15], wherein it is found that the effective structural mass for the purpose of understanding the response of a buried structure to ground shock is made up of both the mass of the buried structure and that of the soil. In fact, they state that the majority of the mass which influences the work done in a buried spring-piston system is contributed by the ground material between it and the charge. However, the magnitude of the initial pressure peak is largely influenced by the mass of the structure alone.

## Conclusions

A numerical model has been developed which effectively captures the displacement of a deformable plate subjected to ground shock loading, as validated by experimental results. DIC has allowed for deformation across a large area of the plate to be captured during explosive tests, which confirms the validity of the LS-DYNA model.

It has been shown that although the shock load is represented effectively, the mass movement of soil is insufficiently captured, resulting in a poor representation of the temporal plate behaviour at larger SODs – even though the peak magnitude is similar. As such, the model can be used effectively to determine near-field loading and response, although requires further work if used for far-field prediction of structural deformation.

In future, this work should be extended to account for the effect of changing charge size (to validate the assumption of cube-root scaling of loading on a structure). Additionally, a greater range of SODs is required to establish the point at which the model no longer suitably characterises the plate behaviour.

## References

[1] Cooke, S. (2015). UNEXPLODED ORDNANCE. *Tunnels & Tunneling International*, 43–46.

[2] Stone, K., Murray, A., Cooke, S., Foran, J., & Gooderham, L. (2009). *Unexploded ordnance (UXO). A guide for the construction industry*. CIRIA.

[3] Lampson, C. W. (1946). *Final report on effects of underground explosions*.

[4] Ingram, L. F. (1972). *Ground Motions from High-Explosive Experiments*.

[5] Ingram, J. K., Drake, J. L., & Ingram, L. F. (1975). *Influence of Burst Position on Airblast, Ground Shock and Cratering in Sandstone*.

[6] Ingram, Leo. F. (1967). *Instrumentation for Earth Stresses and Motions Produced by Explosions*.

[7] van Dongen, Ph., & Weerheijm, J. (1992). Interaction of Ground Shock with Soil Pressure Transducers. In P. S. Bulson (Ed.), *Structures Under Shock and Impact 2* (pp. 625–635).

[8] Wang, X., Li, Y., Zhou, H., Dai, H., & Jayasinghe, L. B. (2020). Accurate measurement of ground shock with cellular solid. *International Journal of Impact Engineering*, *145*. https://doi.org/10.1016/j.ijimpeng.2020.103675

[9] Westine, P. S. (1978). Ground Shock From the Detonation of Buried Explosives. *Journal of Terramechanica*, *15*(2), 69–79.

[10] Westine, P. S., & Friesenhahn, G. J. (1983). *Free-Field Ground Shock Pressures From Buried Detonations In Saturated and Unsaturated Soils*.

[11] Drake, J. L., & Little, C. D. (1983). *Ground Shock From Penetrating Conventional Weapons*.

[12] Drake, J. L., Smith, E. B., & Blouin, S. E. (1989). Enhancements of the Prediction of Ground Shock From Penetrating Weapons. *Proceedings of the Fourth International Symposium on the Interaction of Non-Nuclear Munitions with Structures (Volume 2)*, 7–12.

[13] US Army Engineers Waterways Experimental Station. (1986). TM5-855-1 Fundamentals of protective design for conventional weapons. In *US Army, Navy and Air Force, US Government Printing Office, Washington DC*.

[14] Laine, L., & Larsen, O. P. (2007). Numerical Study of How the Ground Shock Coupling Factor is Influenced by Soil Properties. *78th Shock & Vibration Symposium*.

[15] Laine, L., Johansson, M., & Larsen, O. P. (2015). Simulation of experiments which show that reflection pressure time history from ground shock depends on the reflected structure's stiffness and mass. *86th Shock and Vibration Symposium, Shock and Vibration Exchange*.

[16] Laine, L., Johansson, M., & Larsen, O. P. (2016). 3D FE and 2DOF simulations of ground shock experiments-Reflection pressure time history dependency due to the structure's stiffness and mass. *87th Shock and Vibration Symposium, Shock and Vibration Exchange*.

[17] Laine, L., Johansson, M., & Larsen, O. P. (2018). 2D FE and 2DOF Simulations of Ground Shock Experiments – Total Structure's Spring Energy Displacement Dependency to the Charge's and Structure's Properties. *89th Shock and Vibration Symposium, Shock and Vibration Exchange*.

[18] Hultgren, S. (1979). *Explosion of buried model structures  to buried TNT explosions in sand*.

[19] Shelton, T. W., Ehrgott, J. Q., Moral, R. J., & Barbato, M. (2014). Experimental and numerical investigation of the ground shock coupling factor for near-surface detonations. *Shock and Vibration*, *2014*. https://doi.org/10.1155/2014/789202

[20] Clarke, S., Rigby, S., Fay, S., Barr, A., Tyas, A., Gant, M., & Elgy, I. (2020). Characterisation of buried blast loading. *Proceedings of the Royal Society A: Mathematical, Physical and Engineering Sciences*, *476*(2236). https://doi.org/10.1098/rspa.2019.0791

[21] Waddoups, R., Clarke, S., Tyas, A., Rigby, S., Gant, M., & Elgy, I. (2023). An Approach to Quantifying the Influence of Particle Size Distribution on Buried Blast Loading. *Eng*, *4*(1), 319–340. https://doi.org/10.3390/eng4010020

[22] Laine, L., & Sandvik, A. (2001). DERIVATION OF MECHANICAL PROPERTIES FOR SAND. *4th Asia-Pacific Conference on Shock and Impact Loads on Structures*, 361–368.

[23] Chen, X., Peng, Y., Peng, S., Yao, S., Chen, C., & Xu, P. (2017). Flow and fracture behavior of aluminum alloy 6082-T6 at different tensile strain rates and triaxialities. *PLoS ONE*, *12*(7). https://doi.org/10.1371/journal.pone.0181983

[24] Vedantam, K., Bajaj, D., Brar, N. S., & Hill, S. (2006). Johnson - Cook strength models for mild and DP 590 steels. *CP845, Shock Compression of Condensed Matter*, *845 I*, 775–778. https://doi.org/10.1063/1.2263437